Journal of Nuclear Materials 399 (2010) 87–100

Contents lists available at ScienceDirect

Journal of Nuclear Materials

journal homepage: www.elsevier.com/locate/jnucmat

A general model for predicting coolant activity behaviour for fuel-failure monitoring analysis

A. El-Jaby [a,*], B.J. Lewis [a], W.T. Thompson [a], F. Iglesias [b], M. Ip [c]

[a] Department of Chemistry and Chemical Engineering, Royal Military College of Canada, P.O. Box 17000, Station Forces, Kingston, Ontario, Canada K7K 7B4
[b] Candesco Corporation, 230 Richmond Street West, 10th Floor, Toronto, Ontario, Canada M5V 1V6
[c] Bruce Power, 123 Front Street West, 4th Floor, Toronto, Ontario, Canada M5J 2M2

ARTICLE INFO

Article history:
Received 13 October 2009
Accepted 12 January 2010

ABSTRACT

A mathematical treatment has been developed to predict the release of volatile fission products from operating defective nuclear fuel elements. The fission product activity in both the fuel-to-sheath gap and primary heat transport system as a function of time can be predicted during all reactor operating conditions, including: startup, steady-state, shutdown, and bundle-shifting manoeuvres. In addition, an improved ability to predict the coolant activity of the ^{135}Xe isotope in commercial reactors is discussed. A method is also proposed to estimate both the burnup and the amount of tramp uranium deposits in-core. The model has been validated against in-reactor experiments conducted with defective fuel elements containing natural and artificial failures at the Chalk River Laboratories. Lastly, the model has been benchmarked against a defective fuel occurrence in a commercial reactor.

1. Introduction

On rare occurrences, a fuel element may become defective, allowing high-pressure heavy water (D_2O) coolant to enter the fuel-to-sheath gap and providing a direct path for the release of fission products (mainly volatile species of iodine and noble gases) and fuel debris into the primary heat transport system (PHTS) [1–6]. In addition, the entry of high-pressure D_2O coolant into the gap may cause the UO_2 fuel to oxidize, which in turn will augment the rate of fission product release into the PHTS [7,8]. The release of fission products and fuel debris into the PHTS can elevate circuit contamination levels [1–6]. Moreover, with continued operation of a defective fuel element, the thermal performance of the element can be affected since the thermal conductivity and incipient melting temperature are reduced due to fuel oxidation effects [8]. It is therefore desirable to discharge defective fuel as soon as possible. Hence, a better understanding of defective fuel behaviour is required in order to develop an improved methodology for fuel-failure monitoring and PHTS coolant activity prediction.

Several codes have been previously developed for fuel-failure monitoring in CANDU®[1] reactors [3] and light water reactors (LWRs) [9–11]. More recently, Likhanskii et al. have developed a mechanistic expert system for fuel-failure analysis in water-cooled water-moderated energy reactors (WWERs) [12,13]. Most tools use a steady-state coolant activity analysis [3,9–11], where a Booth diffusion-type model is used to describe the fission product release from the UO_2 fuel matrix into the gap [14,15], and a first-order kinetic model to consider the transport, hold-up, and release of fission products from the gap into the PHTS coolant [3,9–11]. It is therefore necessary to use an empirical diffusion coefficient D' [s^{-1}] to account for fission product diffusion in the UO_2 fuel matrix and an escape-rate coefficient v [s^{-1}] for the release from the gap into the PHTS coolant. However, these parameters are not constant in time as they are influenced by the defect condition, which can deteriorate as a result of secondary sheath hydriding and additional mechanical stresses on the brittle sheath [2,4,5].

With further deterioration of the fuel element sheath, there is less hold-up of fission products in the gap. In addition, it has been shown that the fission product diffusivity is enhanced with continued fuel oxidation [7,8]. Moreover, complex thermalhydraulic effects occur on shutdown as the UO_2 fuel pellets contract and D_2O coolant enters the gap. Furthermore, v is further enhanced due to Nernst ionic diffusion as iodine is dissolved from exposed surfaces (mainly UO_2 fuel and sheath material) with contact by liquid D_2O coolant on reactor shutdown. On the subsequent startup, the expansion of the UO_2 fuel pellets will force liquid D_2O coolant (with dissolved iodine) and any residual noble gas out of the gap, resulting in an additional convective release of fission products. These effects can in fact be modelled via a variable v and D', which specifically requires a time-dependent model.

* Corresponding author. Present address: Physics and Fuel Division, Directorate of Assessment and Analysis, Technical Support Branch, Canadian Nuclear Safety Commission, Government of Canada, P.O. Box 1046, Station B, 280 Slater Street, Ottawa, Ontario, Canada K1P 5S9. Tel.: +1 613 943 4918; fax: +1 613 995 5086.
E-mail address: Ali.El-Jaby@cnsc-ccsn.gc.ca (A. El-Jaby).

[1] CANDU (CANada Deuterium Uranium) is a registered trademark of Atomic Energy of Canada Limited.

0022-3115/$ - see front matter
doi:10.1016/j.jnucmat.2010.01.006

As a further limitation of earlier fission product release computational tools that use a steady-state analysis, it is possible to trade off the effects of v (which characterizes the defect size) against the element linear power P [kW m^{-1}] (which affects diffusivity D'). In addition, a steady-state analysis requires a greater number of isotopes of both noble gases and iodines for a more accurate assessment [3]. Moreover, with on-power refuelling in a CANDU reactor, there is a preponderance of coolant activity data that involves a time-dependent behaviour. Hence, a more general treatment is needed in order to effectively make use of all available data (steady-state and transient), that is applicable in all operating conditions, and which accounts for the changing condition of the defect.

The current work synthesizes all previous theoretical treatments [3,9–11] with the solution of a more general time-dependent model. This model, entitled STAR (Steady-state and Transient Activity Release), is able to specifically predict the fission product activity behaviour in the UO_2 fuel matrix, gap, and PHTS coolant, while respecting the overall fission product mass-balance under all reactor operating conditions. In addition, the current treatment has been further generalized to account for recoil release from fuel debris deposited on PHTS loop surfaces and includes a model describing the transient release behaviour of fission products.

2. Model development

The model consists of generalized time-dependent coupled mass-transport equations governing the fission product inventory in the UO_2 fuel matrix, gap, and PHTS coolant. The model is further developed for variable power and coolant purification histories, which allows it to be matched to coolant activity trends and then used in a prognostic manner to predict coolant activity behaviour as a function of reactor power and coolant purification operations.

As first proposed by Booth, the UO_2 fuel pellets within a fuel element are assumed to be composed of a collection of idealized fuel grains throughout the UO_2 fuel matrix in order to determine the fission product concentration distribution and the diffusional release rate from the UO_2 fuel matrix into the gap [14,15]. The Booth diffusion model for the fission product concentration distribution $C(r,t)$ [atoms m^{-3}] for an idealized fuel grain of radius a [m] at a radius r [m] relative to the centre of the grain at time t [s] is:

$$\frac{\partial C(r,t)}{\partial t} = \frac{D(t)}{r^2}\frac{\partial}{\partial r}\left(r^2\frac{\partial C(r,t)}{\partial r}\right) - \lambda C(r,t) + \frac{F_f(t)y^c}{V_f} \tag{1}$$

where $F_f(t)y^c/V_f$ is the volumetric production from fission. For the specified fission product species, $D(t)$ [m^2 s^{-1}] is the diffusion coefficient in the UO_2 fuel matrix and λ [s^{-1}] is the decay constant. Based on an approximate energy release of 200 MeV per fission for a CANDU fuel element operating at a linear power $P(t)$ [kW m^{-1}], the fission rate $F_f(t)$ [fissions s^{-1}] is [16]:

$$F_f(t) = 1.489\times10^{13}P(t) \tag{2}$$

Moreover, given that the earlier members of the radioactive decay chain are relatively short-lived, the fission source-term is based on the cumulative fission yield y^c [atoms fission^{-1}] of the given fission product. Defining a dimensionless radial variable $\eta = r/a$, and multiplying through by the total UO_2 fuel volume in the element V_f [m^3], Eq. (1) becomes:

$$\frac{\partial u(\eta,t)}{\partial t} = \frac{D'(t)}{\eta^2}\frac{\partial}{\partial \eta}\left(\eta^2\frac{\partial u(\eta,t)}{\partial \eta}\right) - \lambda u(\eta,t) + F_f(t)y^c \tag{3}$$

where $u(\eta,t) = C(r/a,t)V_f$ and $D'(t) = D(t)/a^2$. Here, $u(\eta,t)$ [atoms] is the fission product inventory profile in the UO_2 fuel matrix. Eq. (3) is subject to the initial condition:

$$u(\eta,t) = 0, \quad 0 \leqslant \eta \leqslant 1, \quad t = 0 \tag{4a}$$

and the Neumann (Eq. (4b)) and Dirichlet (Eq. (4c)) boundary conditions:

$$\frac{\partial u(\eta,t)}{\partial \eta} = 0, \quad \eta = 0, \quad t \geqslant 0 \tag{4b}$$

$$u(\eta,t) = 0, \quad \eta = 1, \quad t \geqslant 0 \tag{4c}$$

The diffusional release rate of fission products from the UO_2 fuel matrix $R_{diff}(t)$ [atoms s^{-1}] is derived by applying Fick's law of diffusion to the solution of Eq. (3) (i.e., $u(\eta,t)$) such that:

$$R_{diff}(t) = -3D'(t)\left.\frac{\partial u(\eta,t)}{\partial \eta}\right|_{\eta=1} \tag{5}$$

Equivalently, the diffusional release-to-birth rate ratio $(R/B)_{diff}(t)$ from the UO_2 fuel matrix is:

$$\left(\frac{R}{B}\right)_{diff} = \frac{R_{diff}(t)}{F_f(t)y^c} = -\frac{3D'(t)}{F_f(t)y^c}\left.\frac{\partial u(\eta,t)}{\partial \eta}\right|_{\eta=1} \tag{6}$$

Thus, the time-dependent diffusion equation (Eq. (3)) can be solved by numerical methods subject to the conditions described in Eqs. (4a)–(4c). This solution allows for the computation of $R_{diff}(t)$ (Eq. (5)), which in turn becomes the source term for the mass-balance equation governing the fission product inventory in the gap $N_g(t)$ [atoms]:

$$\frac{dN_g(t)}{dt} = R_{diff}(t) - \lambda N_g(t) - v(t)N_g \tag{7a}$$

subject to the initial condition:

$$N_g(t) = 0, \quad t = 0 \tag{7b}$$

Here, $v(t)$ [s^{-1}] is the escape-rate coefficient characterizing the fission product release rate from the gap of the defective element into the PHTS coolant. This release rate is the source term in the mass-balance equation governing the fission product inventory in the PHTS coolant $N_c(t)$ [atoms]:

$$\frac{dN_c(t)}{d} = v(t)N_g(t) - \lambda N_c(t) - \beta_p(t)N_c(t) \tag{8a}$$

subject to the initial condition:

$$N_c(t) = 0, \quad t = 0 \tag{8b}$$

The parameter $\beta_p(t)$ [s^{-1}] is the purification rate for the PHTS coolant.

2.1. Recoil release from tramp U

Fission product release via the recoil mechanism from tramp U deposits on in-core piping surfaces can be an important contributor to the fission product inventory in the PHTS coolant, especially for short-lived isotopes [17]. Accordingly, a tramp U source term is added to Eq. (8a):

$$\frac{dN_c(t)}{dt} = v(t)N_g(t) - \lambda N_c(t) - \beta_p(t)N_c(t) + R_{rec}^{tr\cdot U}(t)RFP(t) \tag{9}$$

where $R_{rec}^{tr\cdot U}(t) = 1/2F_{tr\cdot U}(t)y^c$ [atoms s^{-1}] is the fission product release rate from the total tramp U in-core and $F_{tr\cdot U}(t)$ [fissions s^{-1}] is the tramp U fission rate [17]. Moreover, in order to account for any changes in $F_{tr\cdot U}(t)$ due to overall reactor power manoeuvres, $R_{rec}^{tr\cdot U}(t)$ is scaled by the relative reactor power parameter $RFP(t)$. The total mass of in-core tramp U m_U [kgU] can be related to $F_{tr\cdot U}(t)$ via [3]:

$$m_U = \frac{F_{tr\cdot U}(t)}{2N_A\psi\langle\phi_T^{core}\rangle} \tag{10}$$

where N_A [atoms mol^{-1}] is Avogadro's number and $\langle\phi_T^{core}\rangle$ [n cm^{-2} s^{-1}] is the volumetrically-averaged thermal neutron flux in-core. The parameter ψ [mol cm^2 kgU^{-1}] takes into account temperature-dependent reactor physics considerations for the fissile nuclides ^{235}U and ^{239}Pu [3]:

$$\psi = \frac{\sqrt{\pi}}{4}\sqrt{\frac{T^\circ}{T}}\sum_{i=^{235}\mathrm{U},^{239}\mathrm{Pu}}\left(\frac{w(B)}{A}g_f(T)\sigma_f(T^\circ)\right)_i \tag{11}$$

where $w(B)$ [g kgU^{-1}] is the specific fissile content as a function of burnup B [MWh kgU^{-1}], A [g mol^{-1}] is the atomic mass number, $g_f(T)$ is the non-1/ν neutron absorption fission factor, and $\sigma_f(T^\circ)$ [cm^2] is the microscopic thermal fission cross-section evaluated at the reference temperature T° = 293.61 K.

The solution of the coupled equations (Eqs. (3), (5), (7a), and (8a)) provides a prediction of both the gap and PHTS coolant inventory as a function of time for variable fuel element linear power $P(t)$, reactor full power $RFP(t)$, and coolant purification operations $\beta_p(t)$. Moreover, the degradation of a defective fuel element is tracked with a time-dependent escape-rate coefficient $\nu(t)$, which can be fit to match observed PHTS coolant activity concentrations for prognostic predictions of the coolant activity behaviour for future reactor operations with the presence of defective fuel.

2.2. Precursor diffusion and neutron absorption effects

A more accurate analysis of the release behaviour of fission products with relatively long-lived precursors (^{132}I and ^{135}Xe) and/or large neutron absorption cross-sections (^{135}Xe) requires that these effects be considered. Eq. (3) can be expanded to account for a parent (p) (Eq. (12a)) and daughter (d) (Eq. (12b)) pair:

$$\frac{\partial u_p(\eta,t)}{\partial t} = \frac{D'(t)}{\eta^2}\frac{\partial}{\partial\eta}\left(\eta^2\frac{\partial u_p(\eta,t)}{\partial\eta}\right) - \lambda_p u_p(\eta,t) + F_f(t)y_p^c \tag{12a}$$

$$\frac{\partial u_d(\eta,t)}{\partial t} = \frac{D'(t)}{\eta^2}\frac{\partial}{\partial\eta}\left(\eta^2\frac{\partial u_d(\eta,t)}{\partial\eta}\right) - (\lambda_d + \sigma_a\phi_T^f(t))u_d(\eta,t) + \lambda_p u_p(\eta,t) + F_f(t)y_d^d \tag{12b}$$

where the decay of the parent isotope $\lambda_p u_p(\eta,t)$ provides for an additional source term for the daughter isotope. Here, σ_a [cm^2] is the microscopic neutron absorption cross-section, $\phi_T^f(t)$ [n cm^{-2} s^{-1}] is the thermal neutron flux in the UO_2 fuel matrix, y_p^c is the cumulative fission yield for the parent, and y_d^d is the direct fission yield for the daughter. Eqs. (12a) and (12b) are subject to the conditions described in Eqs. (4a)–(4c). Moreover, the diffusional release rate (Eq. (5)) from the UO_2 fuel matrix can be expressed separately for the parent (Eq. (13a)) and daughter (Eq. (13b)):

$$R_{diff,p}(t) = -3D'(t)\left.\frac{\partial u_p(\eta,t)}{\partial\eta}\right|_{\eta=1} \tag{13a}$$

$$R_{diff,d}(t) = -3D'(t)\left.\frac{\partial u_d(\eta,t)}{\partial\eta}\right|_{\eta=1} \tag{13b}$$

Similarly, the mass-balance equations governing the fission product inventory in the gap and coolant can also be expressed separately for the parent (Eqs. (14a) and (15a)) and daughter (Eqs. (14b) and (15b)):

$$\frac{dN_{g,p}(t)}{dt} = R_{diff,p}(t) - (\lambda_p + \nu_p(t))N_{g,p} \tag{14a}$$

$$\frac{dN_{g,d}(t)}{dt} = R_{diff,d}(t) + \lambda_p N_{g,p}(t) - (\lambda_d + \sigma_a\phi_T^g(t) + \nu_p(t))N_{g,d} \tag{14b}$$

and

$$\frac{dN_{c,p}(t)}{dt} = \nu_p(t)N_{g,p}(t) - (\lambda_p + \beta_p(t))N_{c,p}(t) + R_{rec,p}^{tr\cdot U}(t)RFP(t) \tag{15a}$$

$$\frac{dN_{c,p}(t)}{dt} = \nu_p(t)N_{g,p}(t) + \lambda_p N_{c,p}(t) - (\lambda_p + \beta_p(t) + f_c\sigma_a\phi_T^{core}(t))N_{c,p}(t) + R_{rec,d}^{tr\cdot U}(t)RFP(t) \tag{15b}$$

where:

$$R_{rec,p}^{tr\cdot U}(t) = \frac{1}{2}F_{tr\cdot U}(t)y_p^c \tag{16a}$$

$$R_{rec,d}^{tr\cdot U}(t) = \frac{1}{2}F_{tr\cdot U}(t)y_d^d \tag{16b}$$

Here, the terms $\sigma_a\phi_T^g(t)$ and $\sigma_a\phi_T^{core}(t)$ account for losses due to neutron absorption in the gap and coolant, respectively. Moreover, the neutron absorption loss in the coolant is scaled by a term f_c to account for the fraction of the PHTS that is in-core (Eq. (15b)).

3. Numerical implementation

An earlier version of the time-dependent model has been previously solved using the COMSOL Multiphysics finite-element commercial software package [18]. The finite-element method used in COMSOL is very proficient at solving complex systems of coupled PDEs and ODEs. Notwithstanding, a more robust, single-purpose tool was needed for use at a nuclear power plant (NPP); hence, a stand-alone code for the model is developed in this work.

A finite-difference variable mesh numerical technique with a sparse-matrix solver can be used to solve the Booth diffusion equation (Eq. (3)). The complete details of the mathematical development and validation of the numerical technique are given in [6]. By augmenting the node density near the grain surface, this formu-

Table 1
Summary of *X*-2 defective fuel experiments.

Experiment (element)	Test (defect) description	Defect size (mm^2)		P (kW m^{-1})	B (MWh kgU^{-1})		Defect residence time (effective full power days)	Fuel loss (g)
		Initial	Final		Initial	Final		
Naturally-defective fuel elements								
FFO-102–2 (A7E)	Re-irradiation of element A7E with through-sheath hydriding at high power and cracked hydride blisters at one end of the element	11	300	67	37	67	19	3.5
FFO-110 (A7A, Phase 1)	Power cycling of element A7A with through-sheath hydriding	~0.5	–	14–26	130	140	281	–
FFO-109-2 (A7A, Phase 2)		–	~0.5	22–38	140	155	300	<0.1
Artificially-defected fuel element								
FFO-103 (A3N)	Twenty-three through-sheath slits in a helical pattern along the sheath (dimensions of each slit 36 mm × 0.3 mm)	272	1490	48	0	18	15	~65

lation allows for an accurate solution to the fission product inventory profile in the UO_2 fuel matrix, as well as the diffusional release rate (Eq. (5)), while maximizing computational efficiency. The finite-difference variable mesh technique is unconditionally stable based on a von Neumann stability analysis. A fourth order Runge–Kutta method is used to solve the first-order mass-balance differential equations governing the fission product inventory in the gap and PHTS coolant. The corresponding C++ executable is capable

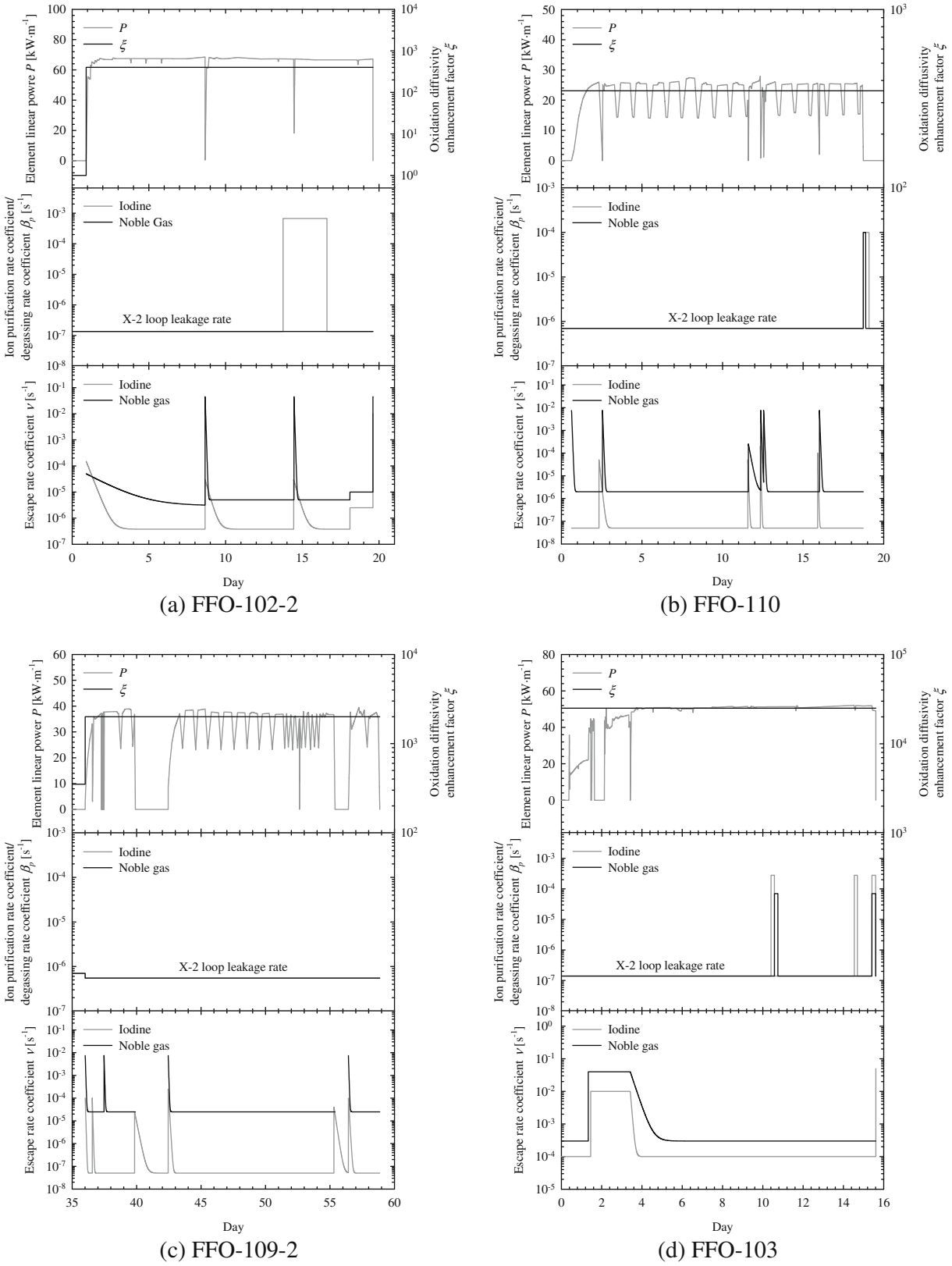

Fig. 1. Input parameters for the analysis of the *X*-2 experiments.

of running on any PC-based platform and the numerical implementation has been extensively benchmarked against the COMSOL numerical solver.

4. Model validation

An extensive experimental programme with defective CANDU-type fuel elements was carried out at the Chalk River Laboratories (CRL) [4]. Fuel elements with various degrees of sheath damage were irradiated in separate tests in the *X*-2 loop of the National Research Experimental (NRX) reactor. A summary of the operational parameters for the X-2 experiments considered in this analysis is detailed in Table 1.

The four *X*-2 experiments selected for the validation of the model cover a range of operating conditions and types of fuel defects. Element A7E represents a severe hydride failure that was initially irradiated in experiment FFO-102-2 at $P = 67$ kW m^{-1} [19,20]. Element A7A incurred a hydride failure that was previously irradiated in experiments FFO-102-1 and FFO-102-3 and then re-irradiated in the power-cycling experiments FFO-110 and FFO-109-2 [21]. Lastly, the artificially defected element A3N (with multiple slits in the sheath) in experiment FFO-103 represents a "worst-case" defect, which was irradiated at $P = 48$ kW m^{-1} [22].

The input parameters of the model analysis of the *X*-2 experiments are based on operational data documented in [19–22]. A Wescott convention flux analysis is used to describe the ^{135}Xe neutron absorption rate in the UO_2 fuel, such that [6]:

$$\sigma_a^{135Xe}\phi_T^f(t) = 7.862\times10^{-5}(P(t)/51) \tag{17a}$$

For the flux analysis in both the gap and core [19]:

$$\sigma_a^{135Xe}\phi_T^{g,core}(t) = 1.963\sigma_a^{135}\mathrm{Xe}\phi_T^f \tag{17b}$$

The effect of burnup on the isotopic yields is not required since the *X*-2 experiments were performed with enriched fuel (5.0 wt.% ^{235}U). Finally, the complicating effect of tramp U release is also not considered since the *X*-2 loop is fitted with graphite filters to remove any fuel debris from the PHTS.

The effective diffusion coefficient $D'(t)$ is derived from a sweep-gas experiment with unoxidized fuel [6]:

$$D'(t)\begin{cases} = \xi(t)e^{(a_0+a_1P(t)+a_2P(t)^2)}, & P > 18 \text{ kW m}^{-1} \\ = \xi(t)e^{(a_0+a_1 18+a_2 18^2)}, & P \leqslant 18 \text{ kW m}^{-1} \end{cases} \tag{18}$$

The parameter $\xi(t)$ is a scaling factor to account for enhanced fission product diffusion due to fuel oxidation effects [6]. Here, $a_0 = -30.856311$, $a_1 = -0.039332$, and $a_2 = 2.05696\times10^{-3}$. The effective diffusion coefficient $D'(t)$ in Eq. (18) is used for both iodine and noble gas species. This coefficient does not take into account effects of fuel cracking during reactor transients since this process is an inefficient release mechanism [23].

The steady-state escape-rate coefficients v_{ss} used in this analysis are based on previous steady-state analyses of the *X*-2 experiments [3]; however, in order to account for any enhanced release during reactor transients in the current application, a variable escape-rate coefficient $v(t)$ is introduced [6]:

$$v(t) = (v_{tr} - v_{ss})e^{-(t/\tau_{ss})} + v_{ss} \tag{19}$$

Here, v_{tr} is the transient (enhanced) escape-rate coefficient and τ_{ss} [s] is a factor which characterizes the relaxation time to steady-state release conditions. This formulation accounts for convective, thermalhydraulic, and pellet expansion/contraction effects which occur during the initial sheath breach and with transient operations. This formulation is able to specifically account for convective release of noble gases during reactor startup and for iodine-spiking phenomenon typically seen during reactor shutdown. Hence, this permits for a continuous transition from the transient to the steady-state release condition.

The model input parameters for the analysis of the *X*-2 experiments are presented in Fig. 1. In each case, an identical $D'(t)$ (and $\xi(t)$) is used for both iodine and noble gas species. Moreover, the same $v(t)$ and $\beta_p(t)$ is applied to each isotope of the same species.

Good agreement is observed between the measured coolant activity concentrations and the model predictions for both the iodine and noble gas species for each *X*-2 experiment. As listed in Table 2, the values of v_{ss} are consistent with previous steady-state analyses [3]. Furthermore, as demonstrated in Figs. 2–5, the application of a more generalized $v(t)$ (Eq. (19)) accounts for the transient release behaviour observed for both iodine and noble gas fission products.

The analysis of the *X*-2 experiments yield a range of values of $D'(t)$ that is consistent with measured diffusion coefficients from intact and defective fuel rods in German BWR and PWR units (Fig. 6) [24]. The exception is for the enhancement factor for FFO-103 ($\xi(t) = 2.5\times10^4$), which is significantly higher. This is due to the high degree of UO_2 fuel oxidation as a result of the relatively large artificially-induced defects of element A3N (Table 1). The fitted values of $D'(t)$ used in this work are also consistent with previous steady-state analyses of the *X*-2 experiments [3].

The current analysis of both the ^{132}I and ^{135}Xe isotopes clearly demonstrates the importance of considering the effects of precursor diffusion. Moreover, the uncertainty behind the behaviour of tellurium during steady-state and transient conditions increases the complexity of the ^{132}I analysis [6]. The analysis of ^{135}Xe is further complicated by losses due to neutron absorption. Notwithstanding, as seen in Figs. 2–5, the predictions are in good agreement with the observed behaviour of these isotopes.

5. Commercial reactor application

5.1. Model input analysis

A systematic assessment of defect exposure in several units of a commercial reactor was carried out in [25]. An analysis of a repre-

Table 2
Evaluation of $v(t)$ for the *X*-2 experiments.

X-2 experiment	P (kW m^{-1})		Steady-state analysis [3]	STAR transient analysis		
			v_{ss} [s^{-1}]	v_{ss} [s^{-1}]	v_{tr} [s^{-1}]	τ_{ss} [s^{-1}]
FFO-102-2	67	I	2.50×10^{-6}	3.75×10^{-7}	3.00×10^{-5}–1.00×10^{-2}	1.81×10^{4}–2.50×10^{4}
		NG	8.40×10^{-6}	3.00×10^{-6}–5.00×10^{-6}	5.00×10^{-5}–4.50×10^{-2}	2.00×10^{3}–1.18×10^{5}
FFO-110	26 (14–26)	I	6.80×10^{-8}	5.00×10^{-8}	5.00×10^{-5}–2.00×10^{-4}	1.43×10^{3}–5.71×10^{3}
		NG	9.30×10^{-7}	2.00×10^{-6}	2.50×10^{-4}–7.50×10^{-3}	2.00×10^{3}–1.00×10^{4}
FFO-109-2	33 (22–38)	I	6.80×10^{-8}	5.00×10^{-8}	2.50×10^{-5}–1.00×10^{-4}	2.00×10^{3}–1.33×10^{4}
		NG	4.90×10^{-5}	2.50×10^{-5}	7.50×10^{-3}	2.00×10^{3}
FFO-103	51	I	1.80×10^{-4}	1.00×10^{-4}	1.00×10^{-2}–5.00×10^{-2}	5.00×10^{3}
		NG	2.30×10^{-4}	3.00×10^{-4}	4.00×10^{-2}	2.00×10^{3}

sentative case (R8Z, Table 3) from this survey is selected for code benchmarking, where a single failure was present in-core. The irradiation history, as well as the purification operations, was determined from historical reactor data. The linear power of the defective element was calculated using the SORO reactor physics code based on the bundle power histories. PHTS coolant activities for ^{131}I, ^{88}Kr, ^{133}Xe, and ^{135}Xe were monitored and collected. The PHTS coolant activity was assessed with grab-sample monitoring from the Chemical Environmental Management (CEM) database and with on-line gaseous fission product (GFP) monitoring from

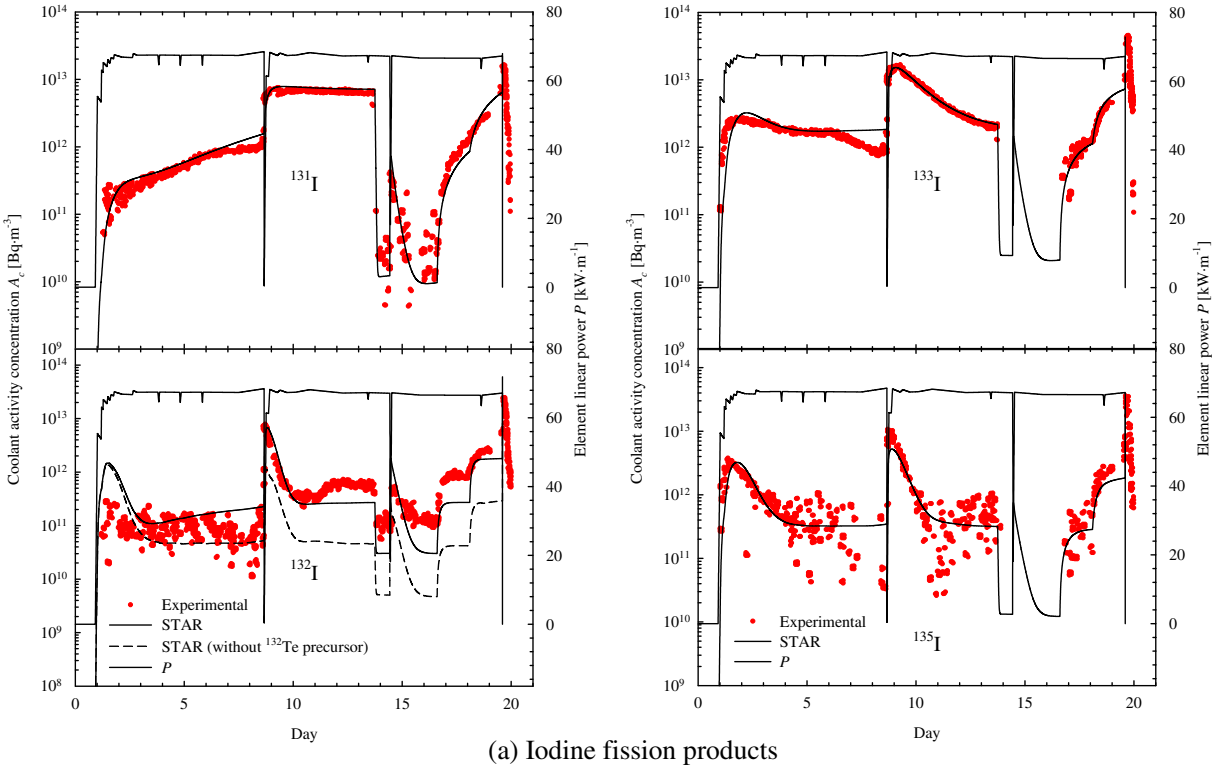

(a) Iodine fission products

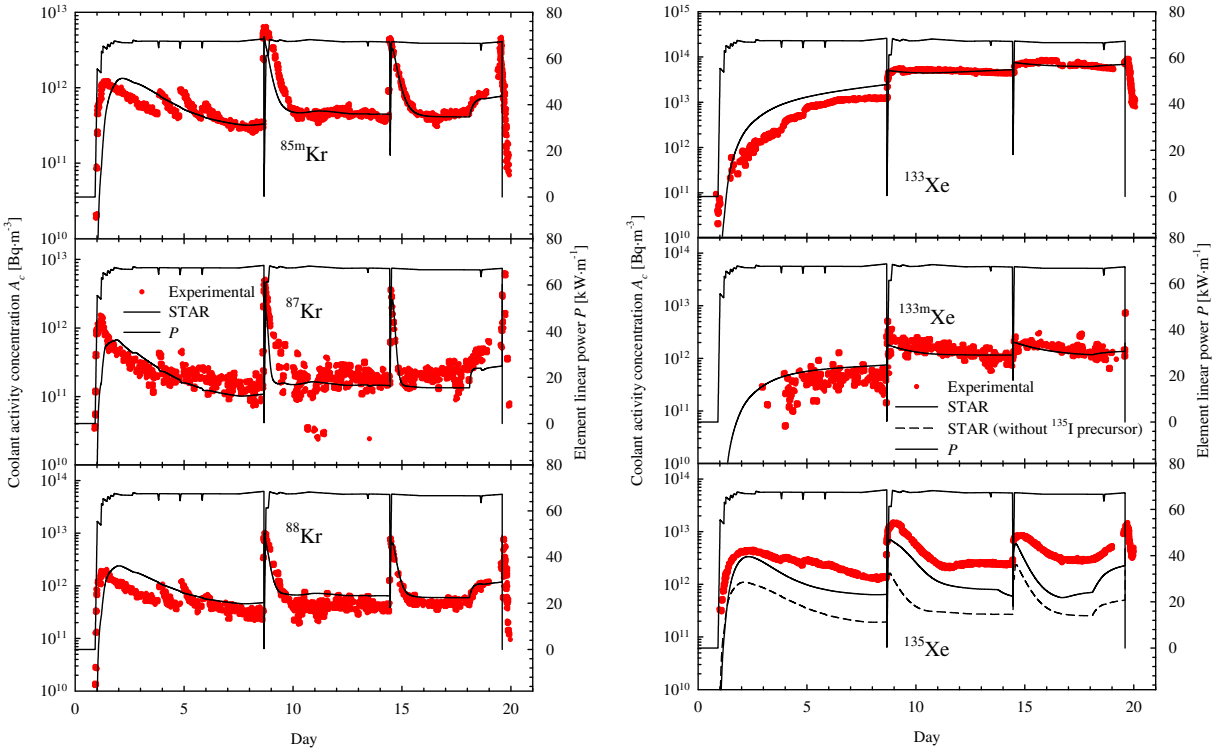

(b) Krypton fission products

(c) Xenon fission products

Fig. 2. Model analysis for *X*-2 experiment FFO-102–2.

the Plant Information (PI) database. Only PHTS coolant activity levels greater than a preset threshold limit for each isotope (based on a total PHTS mass of 2.44×10^5 kg) were stored in the PI database, whereas lower activities were available in the CEM database. Finally, the Fuels Inspection Database (FID) provided inspection results of the defective elements.

Input data for the model is shown in Fig. 8 along with the corresponding escape-rate coefficient $v(t)$. The values of $v(t)$ necessary to reproduce the coolant activity concentrations are consistent with those used in the analysis of the *X*-2 experiments (Table 2). The empirical diffusion coefficient $D'(t)$ used in the analysis of the commercial case is based on Eq. (18), where the oxidation enhancement

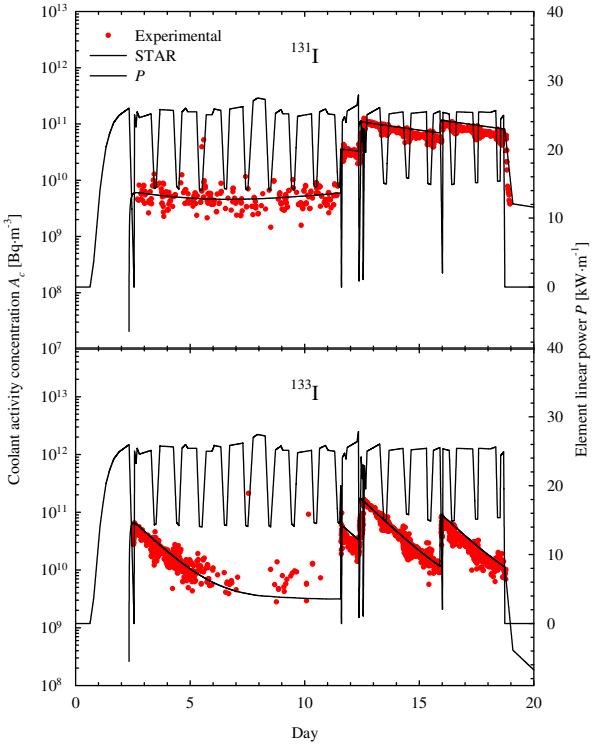

(a) Iodine fission products

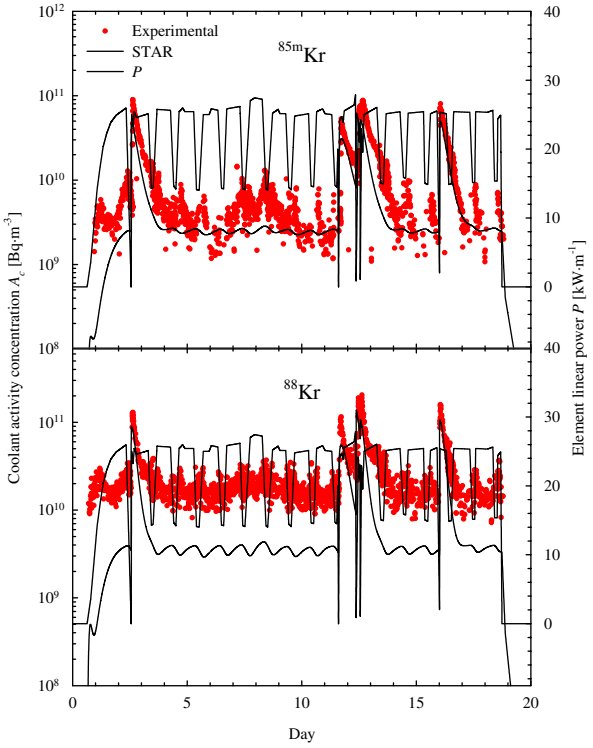

(b) Krypton fission products

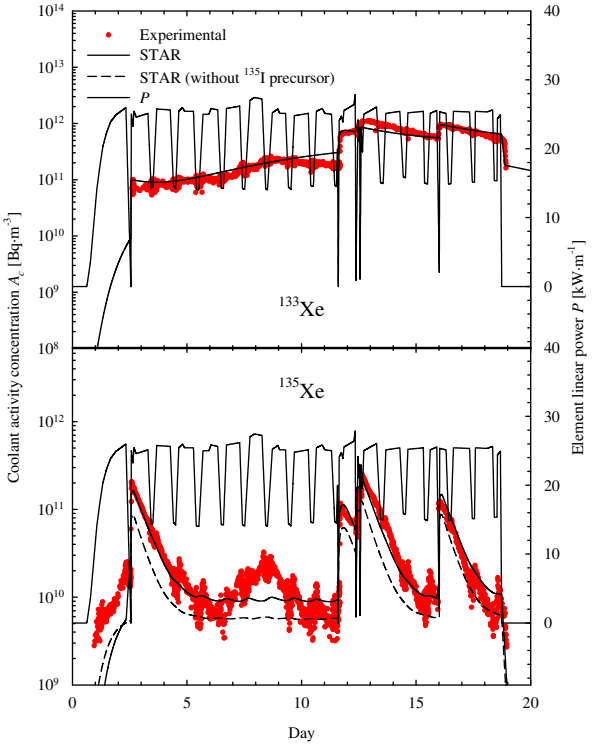

(c) Xenon fission products

Fig. 3. Model analysis for *X*-2 experiment FFO-110.

factor is set to unity ($\xi(t) = 1$) until the time the defect is presumed to occur. Unlike the *X*-2 analysis, one needs to also consider increasing fuel oxidation effects after sheath breach due to the longer post-defect residence time in the commercial reactor. Thus, $\xi(t)$ is considered as both a constant and a linear function of time to better reflect the effect of continued fuel oxidation.

A constant or linear function for $\xi(t)$ did not significantly change the predicted activity concentrations for ^{88}Kr and ^{135}Xe. This is attributed to their short half-lives, which allows the inventory in the gap to quickly reach equilibrium. On the other hand, for the long-lived ^{133}Xe isotope, enhanced diffusivity in the UO_2 fuel matrix strongly affects the time-dependent inven-

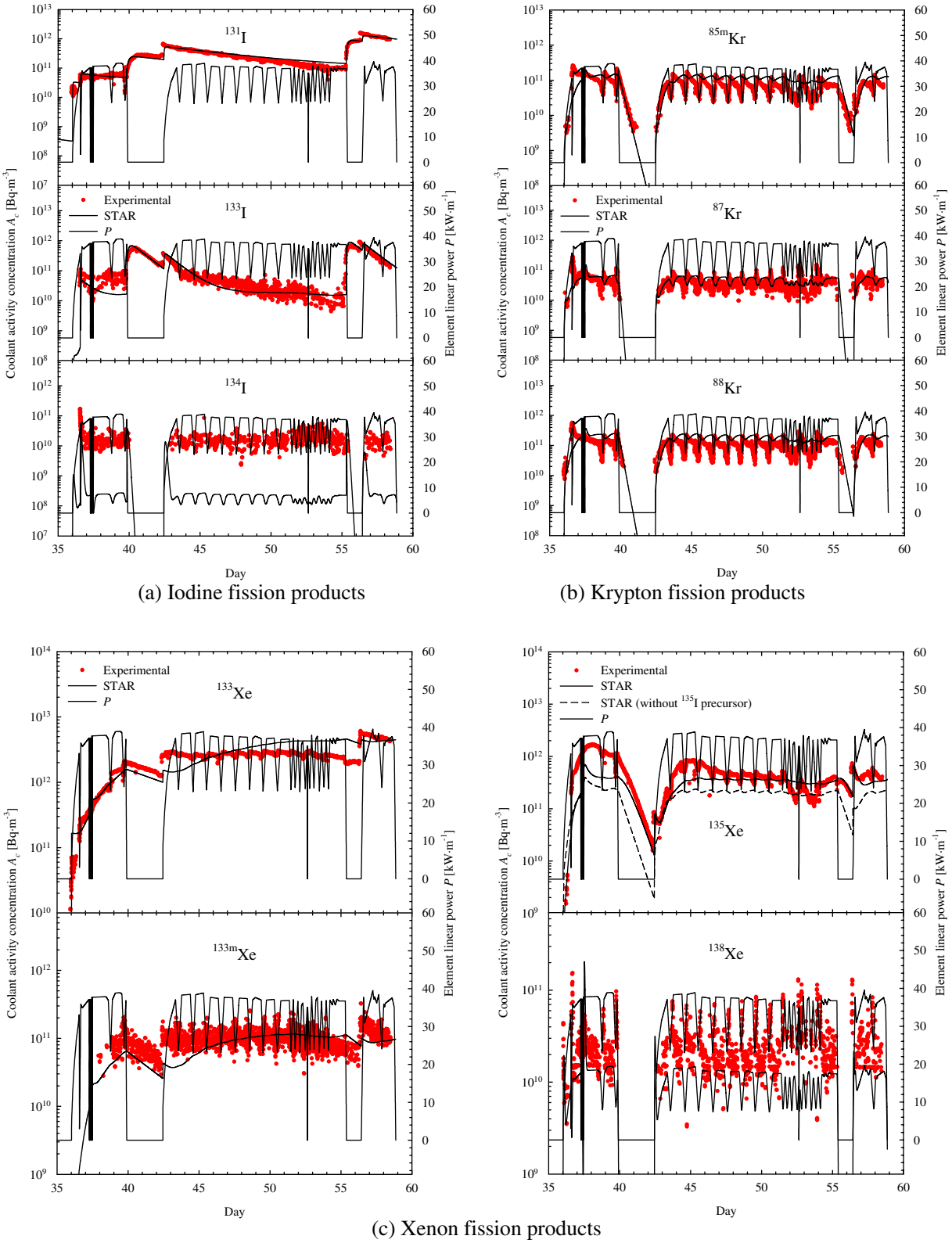

(a) Iodine fission products

(b) Krypton fission products

(c) Xenon fission products

Fig. 4. Model analysis for *X*-2 experiment FFO-109–2.

tory in the gap. For instance, as shown in Fig. 9a, when a constant factor of $\xi = 750$ is used for R8Z, the model over-predicts the ^{133}Xe coolant activity concentration in the early stages because too much release is predicted from the fuel matrix. In contrast, three days before bundle discharge, the model under-predicts the coolant activity level for a constant oxidation factor. This bundle operated at approximately $P = 40\ \mathrm{kW\ m^{-1}}$ when the sheath breach occurred, and it was later discharged 28 days after incurring failure. According to the analysis in [8], the fuel would continually oxidize under these circumstances (Fig. 7), and therefore the use of a linear function is needed for a more accurate prediction.

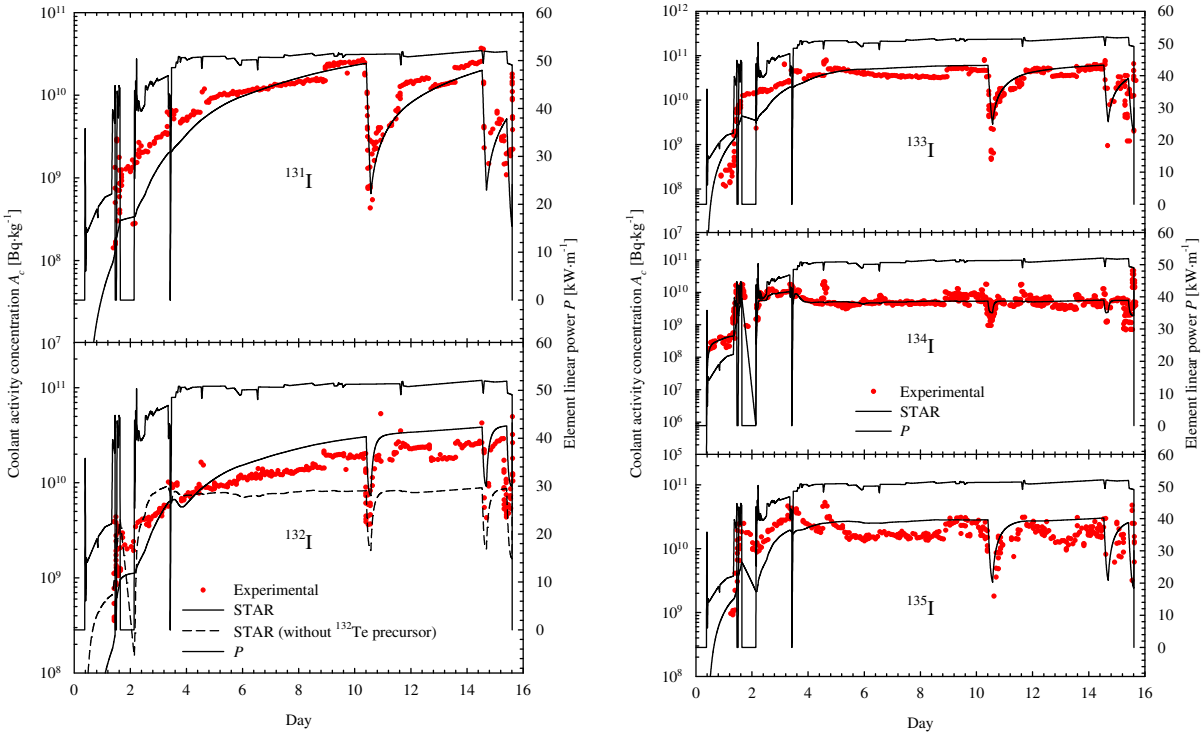

(a) Iodine fission products

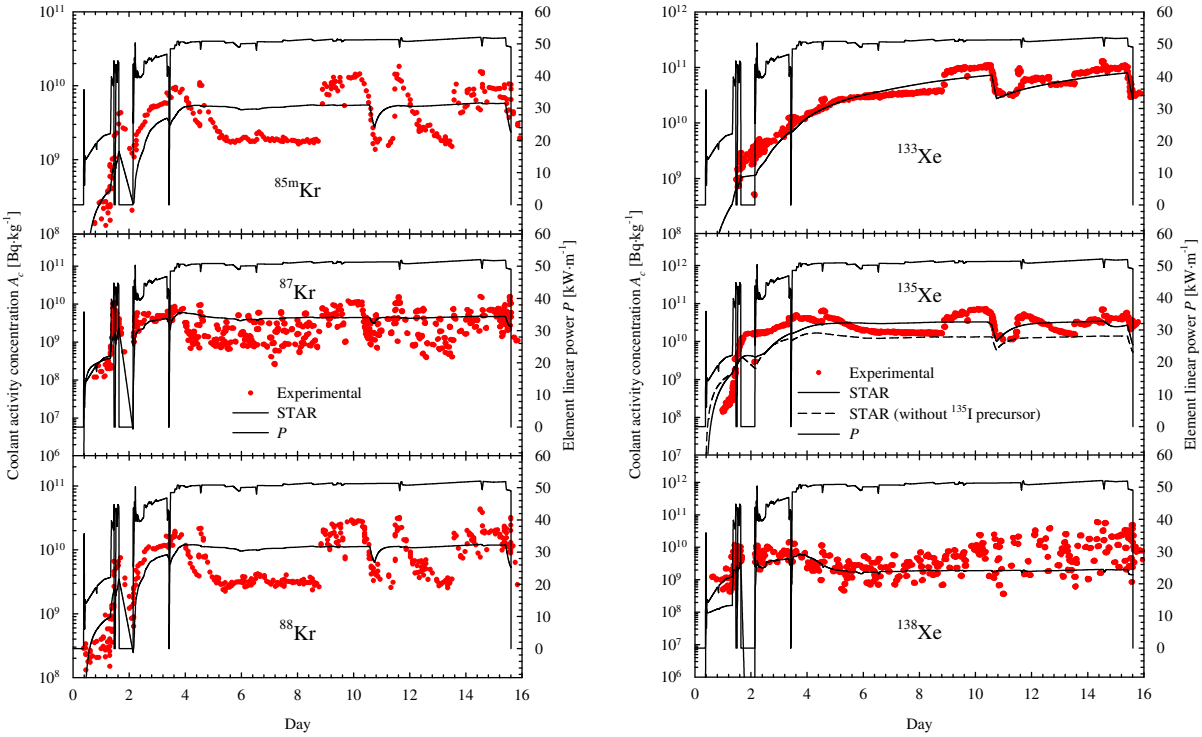

(b) Krypton fission products

(c) Xenon fission products

Fig. 5. Model analysis for *X*-2 experiment FFO-103.

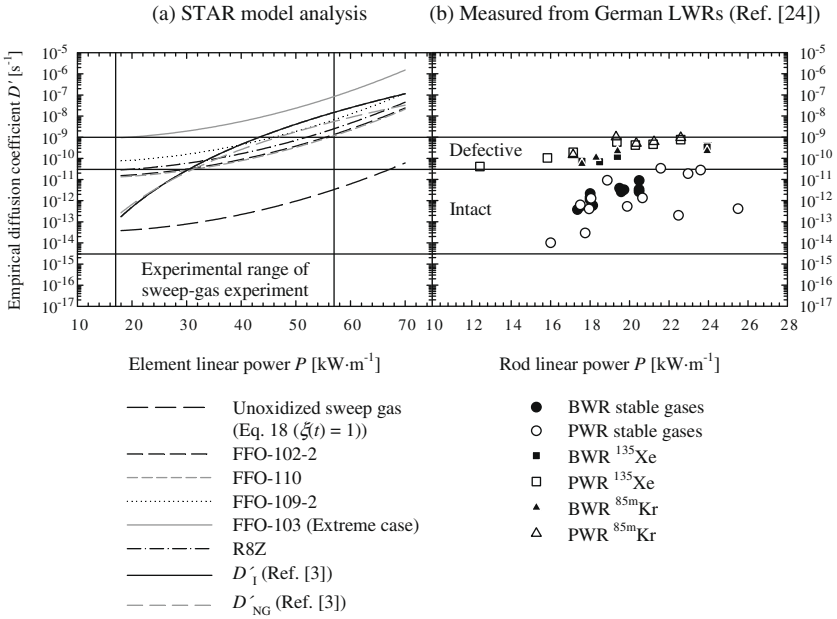

Fig. 6. Empirical diffusion coefficient as a function of element/rod linear power.

Table 3
Details of the commercial defect R8Z.

Case	Date (channel/bundle position)		Fuel shift dates (channel/bundle position)		Time of sheath breach	Defect description	
	Loading	Discharge	Shift 1	Shift 2		Primary cause	Examination details
R8Z	20-Nov-1999 (M03/01)	8-May-2000 (M03/13)	13-Mar-2000 (M03/04)	7-May-2000 (M03/13)	Day 99	Incomplete end-cap weld	Broken hydride blister (5 mm in diameter)

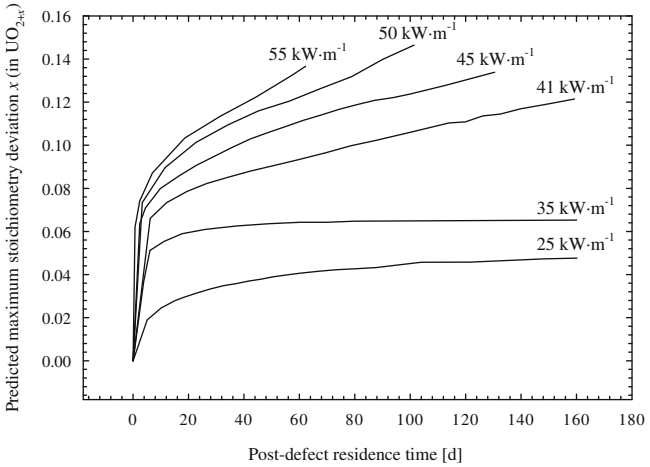

Fig. 7. UO_2 fuel oxidation model predictions of the maximum stoichiometry deviation x (in UO_{2+x}) of a typical commercial defective CANDU fuel element [8].

The values of the escape-rate coefficient necessary to reproduce the coolant activity concentration in the commercial analysis of R8Z are consistent with those of the *X*-2 experiments.

Commercial CANDU fuel elements contain natural fuel, thus the effects of burnup on the isotopic yields, especially for the krypton species, must be considered as the plutonium contribution builds up. A typical average burnup of $B = 100$ MWh kgU^{-1} is assumed over the entire irradiation period for the given analysis.

The noble gas measurements exhibited a sudden drop at day 118. Shortly thereafter, the coolant activity concentration returned to previous levels. This feature is indicative of a degassing operation, which is modelled with a degassing rate coefficient of $\beta_p = 1 \times 10^{-5}$ s^{-1} from day 118.08 to 118.40.

5.1.1. ^{135}Xe considerations

Several assumptions have to be made for the ^{135}Xe analysis. It is difficult to assess *a priori* the thermal neutron flux in the core $\phi_T^{core}(t)$, gap $\phi_T^g(t)$, and UO_2 fuel $\phi_T^f(t)$, required in Eqs. (12b), (14b), and (15b). The commercial reactor has a maximum thermal neutron flux in the fuel of $\phi^f_{T,\max} = 1.15 \times 10^{14}$ n cm^{-2} s^{-1}, with a radial average-to-maximum factor 0.85 and an axial average-to-maximum factor of 0.649 [6]. Hence, the volumetrically-averaged thermal neutron flux in the fuel can be determined as [6]:

$$\langle \phi_T^f \rangle = (1.15 \times 10^{14}) \times (0.85) \times (0.649) \times RFP(t) \tag{20}$$

which is scaled to the relative reactor full power $RFP(t)$. Given $\langle \phi_T^f \rangle$, it is possible to determine the thermal neutron flux at the fuel pellet surface $\phi_T^f(r = a)$ for a specified wt.% ^{235}U enrichment and fuel burnup B. For a CANDU-type pellet diameter $2a = 1.215$ cm and 0.71 wt.% ^{235}U enrichment at a burnup of $B = 100$ MWh kgU^{-1}, the flux depression from the UO_2 fuel surface to the volumetrically-averaged value is [6,26]:

$$\frac{\phi_T^f(r = a)}{\langle \phi_T^f \rangle} = 1.6069 \tag{21}$$

The thermal neutron flux in the UO_2 fuel matrix can be approximated as the volumetrically-average value where $\phi_T^f(t) = \langle \phi_T^f \rangle$.

Table 4
^{135}Xe neutron absorption parameters.

Temperature (K)	$g_a^{135\text{Xe}}$	$\sigma_a^{135\text{Xe}}$ (cm^2)
293.61	1.1581	2.6476×10^{-18}
519.00	1.2341	2.1763×10^{-18}
1228.00	0.9028	1.0350×10^{-18}

Table 5
Tramp U analysis for R8Z.

Input data		Tramp U analysis results	
$A_c^{88\text{Kr}}$ (Bq)	2.03×10^{10}	B (MWh kgU^{-1})	141
A_c^{Xe133} (Bq)	5.87×10^{10}	$F_{tr.U}$ (fissions s^{-1})	1.90×10^{12}
$\langle\phi_T^{core}\rangle$ (n cm^{-2} s^{-1})	9.17×10^{13}	m_U [gU]	3
RFP	0.899		

Moreover, the thermal neutron flux in the gap $\phi_T^g(t)$ and core $\phi_T^{core}(t)$ can be further approximated as the flux at the fuel surface:

$$\phi_T^g(t) = \phi_T^{core}(t) = \phi_T^f(r = a, t) = 1.6069\langle\phi_T^f\rangle \tag{22}$$

These approximations will necessarily give rise to some uncertainty in the ^{135}Xe predictions. Moreover, the additional effect of temperature on the ^{135}Xe neutron absorption cross-section $\sigma_a^{135\text{Xe}}(T)$ must be taken into further consideration. The bulk of the neutron absorption occurs in the UO_2 fuel since only a fraction of the PHTS coolant is in-core, i.e., 2.8%. An average UO_2 fuel temperature of 1228 K can be assumed in the current analysis (for an average core temperature of 519 K) [27]. The temperature dependence of the ^{135}Xe neutron absorption cross-section is described by:

$$\sigma_a^{135\text{Xe}}(T) = \frac{\pi}{2} g_a^{135\text{Xe}}(T)\sqrt{\frac{T^\circ}{T}}\sigma_a^{135\text{Xe}}(T^\circ) \tag{23}$$

where the non-1/v absorption factor $g_a^{135Xe}(T)$ and corresponding $\sigma_a^{135Xe}(T)$ for these given temperatures is listed in Table 4. This effect is also considerable given that $\sigma_a^{135Xe}(T)$ is reduced by a factor of two as the temperature is increased from 519 K to 1228 K.

Finally, another factor that must be considered is the effect of ion purification on the inventory of ^{135}I. Although ion purification removes the iodine fission product from the PHTS loop, it does not inhibit the radioactive decay of this species to its noble gas daughter, ^{135}Xe. With decay, this now becomes a source of noble gases from the ion exchange columns into the PHTS coolant. Thus, to take this additional source into consideration, it is further assumed that ion purification operations have no effect on the loss of ^{135}I for the calculation of the ^{135}Xe coolant activity concentration.

5.1.2. Tramp U analysis

Using observed coolant activity concentrations prior to the presumed time of sheath failure, it is possible to estimate both the burnup B and fission rate $F_{tr.U}(t)$ of the tramp U deposits. The measured noble gas (^{88}Kr and ^{133}Xe) coolant activity concentration prior to the time of failure can be assumed to be at a steady-state condition, whereby this activity is simply equal to the release rate from the tramp U deposits:

$$\frac{1}{2}F_{tr.U}(t)y^{c,\,^{88}Kr}(B)RFP(t) = \left(\lambda^{^{88}Kr} + \beta_p(t)\right)N_c^{^{88}Kr}(t) \approx A_c^{^{88}Kr}(t) \tag{24a}$$

$$\frac{1}{2}F_{tr.U}(t)y^{c,\,^{133}Xe}(B)RFP(t) = \left(\lambda^{^{133}Xe} + \beta_p(t)\right)N_c^{^{133}Xe}(t) \approx A_c^{^{133}Xe}(t) \tag{24b}$$

Here, the degassing rate coefficient $\beta_p(t)$ is zero since no degassing is expected to take place prior to element failure. Converting the measured coolant activity concentrations into an activity [Bq], one can solve for the burnup as the tramp U fission rate must be the same for both ^{88}Kr and ^{133}Xe. This calculation is possible because the fission yield is a function of burnup for the un-enriched fuel [3,6]:

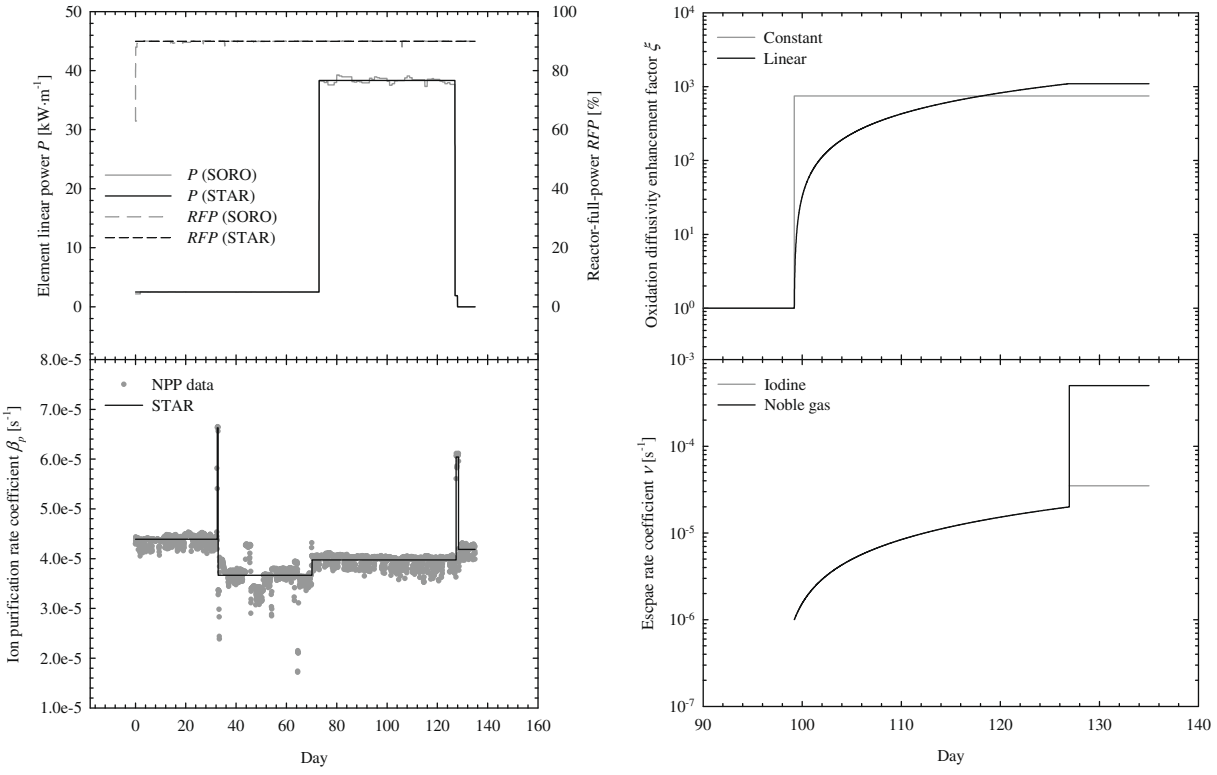

Fig. 8. Model input parameters for the commercial case.

$$y^{c}(B) = \frac{y^{c,^{235}U} w^{^{235}U}(B)\sigma_f^{^{235}U}(E^{\circ}) + y^{c,^{235}Pu} w^{^{235}Pu}(B)\sigma_f^{^{235}Pu}(E^{\circ})}{w^{^{235}U}(B)\sigma_f^{^{235}U}(E^{\circ}) + w^{^{235}Pu}(B)\sigma_f^{^{235}Pu}(E^{\circ})} \quad (25)$$

Here, the specific fissile content $w(B)$ is also a function of burnup and is given by the following expressions for ^{235}U (Eq. (26a)) and ^{239}Pu (Eq. (26b)) [3,6]:

$$w^{^{235}U}(B) = 10^{(0.85095-0.0027604B)} \quad (26a)$$

$$w^{^{239}Pu}(B) = 4.20353\times10^{-3} + 4.0752\times10^{-2}B - 2.9702\times10^{-4}B^2 + 1.3035\times10^{-6}B^3 - 3.18147\times10^{-9}B^4 + 3.22097\times10^{-12}B^5 \quad (26b)$$

With the calculation of the tramp U burnup, it is then possible to determine $F_{tr.U}(t)$ with Eq. (24a) or (24b), and finally the amount of tramp U with Eq. (10). The results of this analysis are summarized in Table 5. Here, the volumetrically-averaged in-core thermal neutron flux is assumed to be $\langle\phi_T^{core}\rangle = 1.6069\langle\phi_T^{f}\rangle$. Previous analyses have indicated typical values of 3–6 g of tramp U in-core [3,4]. As shown in Table 5, the current tramp U analysis is consistent with this observation [3,4].

6. Discussion

6.1. Comparison of model predictions to measurements

As shown in Fig. 9, excellent agreement is seen between the measured coolant activity concentrations for the monitored isotopes ^{131}I, ^{88}Kr, ^{133}Xe, and ^{135}Xe, and the model predictions. The model is also able to predict "iodine-spiking" phenomena characteristic during bundle shifting and reactor shutdown operations. An enhanced release of noble gases is also successfully mod-

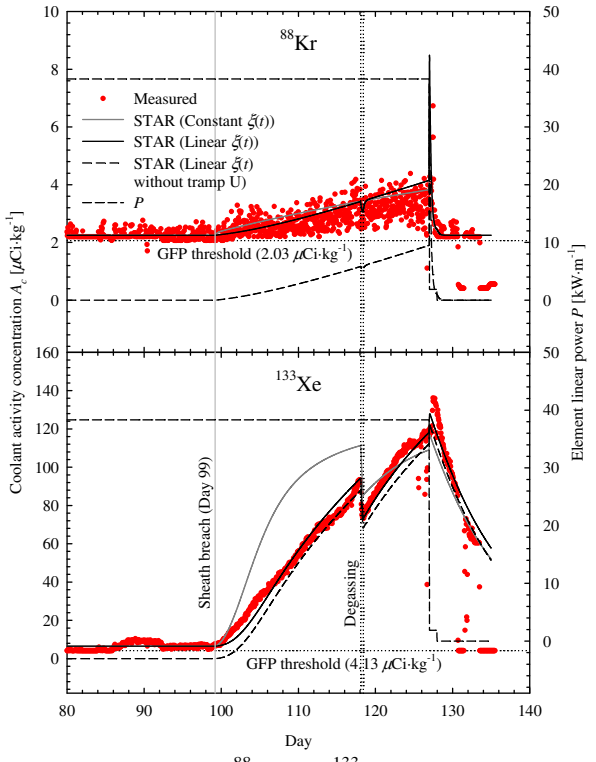

(a) ^{88}Kr and ^{133}Xe

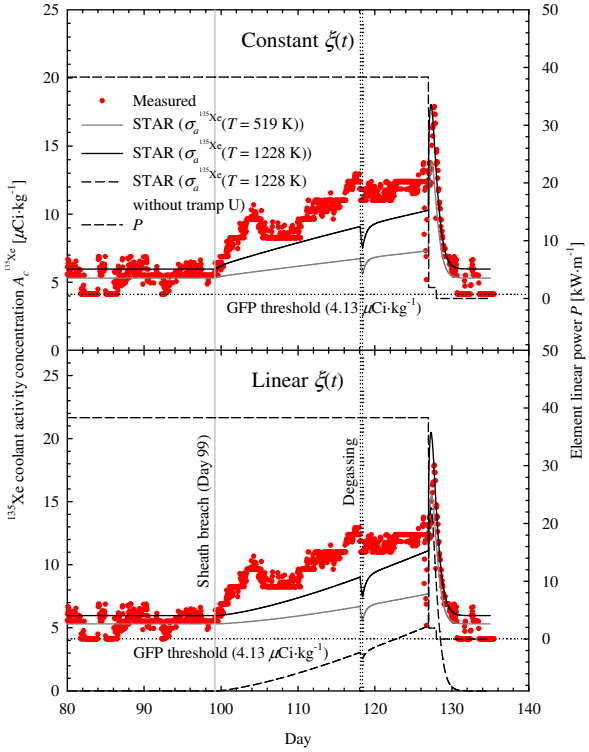

(b) ^{135}Xe

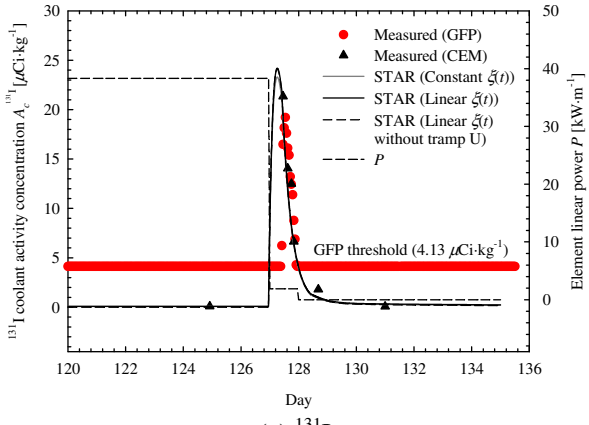

(c) ^{131}I

Fig. 9. Model analysis of the commercial case.

elled during transient conditions. However, unlike the noble gas behaviour in the *X*-2 experiments, an enhanced noble gas release is also observed during reactor shutdown for the commercial defect, most likely due to the horizontal orientation of the CANDU fuel channel. On the other hand, enhanced releases for the noble gases only occurred on startup with the vertically-oriented elements in the NRX reactor of the *X*-2 loop facility at CRL. In the latter case, noble gases are trapped at the top of the element depending on the location of the defect. Lastly, as observed in Fig. 9, the effect of the recoil release source term from tramp U deposits significantly impacts the predictions of the shorter-lived ^{88}Kr but, is of less importance for the longer-lived isotopes.

The analysis of ^{135}Xe proved to be much more complex than that of ^{131}I, ^{88}Kr, and ^{133}Xe for the commercial analysis because of precursor diffusion and neutron absorption effects. Nevertheless, the model predictions are able to capture the observed behaviour, despite the necessity of the approximations. A better understanding of the in-core flux distribution and the coolant activity behaviour of the ^{135}I precursor would improve this analysis but, this level of detail is typically not known for fuel-failure monitoring applications at the NPP.

A marked difference between the *X*-2 defect experiments and commercial defect occurrences is that the latter exhibited continuously increasing noble gas coolant activity concentrations. This is indicative of a deteriorating defect (increase in size) due to hydriding after the initial breach. This translates into a continuously increasing $v(t)$, as depicted in Fig. 8. The coolant activity concentration did not reach a steady-state level before shutdown (fuel bundle discharge), where the entire noble gas gap inventory was released into the PHTS coolant as a consequence of defect deterioration and coolant entry upon shutdown.

The iodine release on bundle discharge is consistent with "iodine-spiking" phenomena observed in the *X*-2 defect experiments, which was appropriately modelled with Eq. (19) (Fig. 9c).

6.2. Application to non-CANDU reactors

The fuel-failure monitoring tools for CANDU reactors [3], as well as for American [9,10] and French [11] LWRs, use essentially the same Booth diffusion-type model coupled to a first-order kinetic model to the describe the release of fission products from defective fuel. Moreover, the parameters which describe the key processes, such as diffusivity D' and the release of fission products from the gap v, are physically identical. Thus, the generalization of the transport equations presented in this paper would, by extension, apply similarly to the LWR systems described in [9–11]. However, given the differences in design and operational practice between CANDU reactors and LWRs, the values of the transport parameters may differ somewhat (especially the gap escape-rate coefficient v due to the much longer LWR fuel rod design).

7. Conclusions

1. The STAR code is a general time-dependent fission product release model to predict coolant activity behaviour of volatile fission products (namely iodine and noble gas species) during both steady-state and transient reactor operating conditions. The fission product transport model is based on solid-state Booth diffusion in the UO_2 fuel matrix and a first-order kinetics treatment in the fuel-to-sheath gap. The effect of precursor diffusion and neutron absorption, and the loss of fission products by radioactive decay and coolant purification (i.e., ion exchange and degassing operations) have also been incorporated into the model. Furthermore, the analysis of the ^{135}Xe isotope in commercial reactors has been advanced with additional reactor physics and operational considerations taken into account. Finally, a method to approximate both the burnup and the amount of tramp U deposits in-core, as well as the tramp U fission rate, has been proposed for a commercial application.
2. The model has been validated against an extensive set of well-characterized in-reactor experiments with defective elements conducted in the *X*-2 defect loop facility at CRL. The model has been further benchmarked against a defect occurrence in a commercial reactor where a single failure was known to be present.

Acknowledgements

The authors would like to acknowledge the assistance and support of the Nuclear Safety Analysis and Support Department of Bruce Power. The authors also acknowledge the data made available under the joint Atomic Energy of Canada Limited/Ontario Hydro *X*-2 Defective Fuel Programme. Finally, the authors acknowledge the funding and support of the Natural Sciences and Engineering Research Council of Canada, the CANDU Owner's Group, the Defence Research and Development Branch, and the Royal Military College of Canada.

References

[1] B.J. Lewis, C.R. Phillips, M.J.F. Notely, Nucl. Technol. 73 (1986) 72.
[2] B.J. Lewis, J. Nucl. Mater. 160 (1988) 201.
[3] B.J. Lewis, R.J. Green, W.T. Che, Nucl. Technol. 98 (1991) 307.
[4] B.J. Lewis, R.D. MacDonald, N.V. Ivanoff, F.C. Iglesias, Nucl. Technol. 103 (1993) 220.
[5] B.J. Lewis, A. El-Jaby, J. Higgs, W.T. Thompson, F.C. Iglesias, R. Laidler, J. Armstrong, R. Stone, R. Odunton, J. Nucl. Mater. 366 (2007) 37.
[6] A. El-Jaby, A Model for Predication Coolant Activity Behaviour for Fuel-failure Monitoring Analysis, Ph.D. Thesis, Royal Military College of Canada, March 2009.
[7] B.J. Lewis, F.C. Iglesias, D.S. Cox, E. Gheorghiu, Nucl. Technol. 92 (1990) 353.
[8] J.D. Higgs, B.J. Lewis, W.T. Thompson, Z. He, J. Nucl. Mater. 366 (2007) 99.
[9] C.E. Beyer, Methodology Estimating Number of Failed Fuel Rods and Defect Size, Electric Power Research Institute, EPRI NP-6554, September 1989.
[10] C.E. Beyer, An analytical model for estimating the number and size of defected fuel rods in an operating reactor, in: Proceedings of the American Nuclear Society International Topical Meeting on LWR Fuel Performance, Avignon, France, April 21–24, 1991, p. 437.
[11] D. Parrat, J.B. Genin, Y. Musante, C. Petit, A. Harrer, Failed rod diagnosis and primary circuit contamination level determination thanks to the DIADEME code – fuel failures in water reactors: causes and mitigation, in: Proceedings of a Technical Meeting held in Bratislava, Slovakia, 17–21 June, 2002, IAEA-TECDOC-1345, Part II, p. 265.
[12] V. Likhanskii, I. Evdokimov, O. Khoruzhii, A. Sorokin, V. Novikov, Modelling of fission product release from defective fuel rods under WWER operating conditions and in leakage tests during refueling, in: Proceedings of the 2004 International Meeting on LWR Fuel Performance, Orlando, Florida, September 19–22, 2004, Paper 1083.
[13] V.V. Likhanskii, I.A. Evdokimov, A.A. Sorokin, A.G. Khramov, V.D. Kanukova, O.V. Apollonova, A.V. Ugryumov, WWER Expert system for fuel failure analysis using data on primary coolant activity, in: Proceedings of the 2007 International LWR Fuel Performance Meeting, San Francisco, California, September 30–October 3, 2007, Paper 1067.
[14] A.H. Booth, A Suggested Method for Calculating the Diffusion of Radioactive Rare Gas Fission Products from UO_2 Fuel Elements and a Discussion of Proposed In-Reactor Experiments that may be used to Test its Validity, Atomic Energy of Canada Limited, 1957 [DCI-27 AECL-700].
[15] A.H. Booth, A Method for Calculating Fission Gas Diffusion from UO_2 Fuel and its Application to the X-2-f Loop Test, Atomic Energy of Canada Limited, 1957 [CRDC-721].
[16] B.J. Lewis, A. Husain, J. Nucl. Mater. 312 (2003) 81.
[17] B.J. Lewis, J. Nucl. Mater. 148 (1987) 28.
[18] B.J. Lewis, A. El-Jaby, J. Higgs, W.T. Thompson, F.C. Iglesias, R. Laidler, J. Armstrong, R. Stone, R. Oduntan, J. Nucl. Mater. 366 (2007) 37.
[19] D.F. Shields, E.P. Penswick, R.D. Delaney, B.J. Lewis, Y.H. Kang, D.D. Semeniuk, Irradiation and Gamma-ray Spectroscopy Data for the High-powered, Porous End Plug Defect Experiment FFO-102-2, Atomic Energy of Canada Limited Report, Exp-FFO-10226, April 1982.
[20] B.J. Lewis, Behaviour of a Zircaloy-sheathed UO_2 Fuel Element Containing a Porous End Plug Defect and Exhibiting Secondary Sheath Hydriding Irradiated in Pressurized Light Water at a Linear Power of 67 kW/m, Chalk River Nuclear Laboratories Report CRNL-2473, 1983.

[21] R.L. da Silva, The Irradiation Performance of a Naturally Defective CANDU UO2 Fuel Element Power Cycled Between Linear Powers of 25–14 kW/m and 38–22 kW/m in the *X*-2 Loop of NRX, Chalk River Nuclear Laboratories Report CRNL-2674, September 1984.
[22] R.L. da Silva, The Irradiation of a CANDU UO_2 Fuel Element with Twenty-three Machined Slits Cut Through the Zircaloy Sheath, Atomic Energy of Canada Limited Report AECL-8260, September 1984.
[23] B.J. Lewis, R.D. MacDonald, H.W. Bonin, Nucl. Technol. 92 (1990) 315.
[24] E. Shuster, F. Garzarolli, A. Kersting, K.H. Neeb, H. Stehle, Nucl. Eng. Des. 64 (1981) 81.
[25] R. Oduntan, F. Iglesias, R. Stone, J. Armstrong, B.J. Lewis, Using on-line monitoring of fission product data to manage reactor operations with in-core failed fuel elements, in: Proceedings of the Ninth International Conference on CANDU fuel, Belleville, Ontario, 18–21 September 2005.
[26] M.J.F. Notely, Nucl. Technol. 44 (1979) 445.
[27] K. Shaheen, A Semi-empirical Oxidation Model for Defective Nuclear Fuel, M.Sc. Thesis, Royal Military College of Canada, April 2008.